

STRUCTURAL DEFORMATION SURVEY A CASE STUDY OF OBASANJO LIBRARY COMPLEX THE FEDERAL POLYTECHNIC DAMATURU YOBE STATE, NIGERIA

Umar Barde, Ishaku Iliyasu and Mohammed Mohammed Daki

Department of Surveying and Geoinformatics

The Federal Polytechnic Damaturu, Yobe State Nigeria

E-mail: Wuyo81@yahoo.com

Abstract

The subsidence survey being one for accurate measurement of the movement of building or structure in order to undertake a visual inspection with the aim of assessing the extent and seriousness of the movement and damage of the structure (J.F.A 1992). This become necessary considering how the structure (Obasanjo library complex) is gradually changing and experiencing cracks hence the need to monitor the structure. The periodic monitoring combined both conventional survey (trigonometric heightening) and satellite (global positioning system) where level, electronic theodolite as well as global navigation satellite system receiver was used to determine the external movement of the structure, the acquired data was processed the result revealed that the average height observed of the North, South and East of the building (study area) is relatively same because the most probable value, standard deviation and standard error are almost the same as 9.052, 0.00821 and 0.0055 respectively. Only in the case of Western part that is a little bit different as the most provable value (MPV), standard deviation (SD) and standard error (SE) are 9.0384, 0.02232 and 0.0082 which indicate a little sink of 0.014m height, 0.014m MPV and 0.0027m standard error.

However, at a fitted trend equation of $Y_t = 9.0477 - 0.00031^x t$. The trend analysis plot revealed that the variables such as Actual, Fits and Forecast has an average accuracy of 0.0074075 mean absolute percentage error (MAPE), 0.0006704 Mean absolute deviation (MAD) and 0.000012 Mean square deviation (MSD).

Keywords: Structural, Deformation, Survey.

1.0 INTRODUCTION

The deformation monitoring (also referred to as deformation survey) is a systematic measurement and tracking of the alteration in the shape or dimension of an object as a result of stresses included by applied loads (Uren, J. and Price, W.F. 1994). The deformation monitoring is a major component of logging measured values that may be used for further computation, deformation analysis, predictive maintenance and alarming (J.F.A Moore 1992).

Deformation monitoring is primarily related to the field of applied surveying, but may also be related to civil engineering, mechanical engineering, construction and geology. The measuring devices used for deformation monitoring depend on the application, the chosen method and the preferred measurement interval. The library complex was constructed over two decades and there structure experiencing lots of cracks and becoming a topic of discussion of a community on that it experiences sink etc. it in view of this that the Subsidence is frequently linked to intense faulting and opening of fissures in urban areas, generating a significant geologic hazard that needs to be accurately assessed and monitored (Ferretti, A., Novali, F., Bürgmann, R., Hilley, G., Prati, C. 2004; Mazzotti, S., Lambert, A., Van der Kooij, M., Mainville, A. 2009; Brunori CA, Bignami C, Albano M, Zucca F, Samsonov S, Gropelli G, Norini G, Saroli M, Stramondo S. 2015), Recent researches have demonstrated the applicability of Global Positioning System (GPS) techniques to precisely determine the 3-D coordinates of moving points in the field of natural

hazards such as earthquakes, landslides, and volcanic activity. Indeed, the detailed analysis of the motion of a landslide, in particular for a near real-time warning system, requires the combination of accurate positioning in three dimensions (infracentimetric) and fine temporal resolution (hourly or less) (Malet, J. P., Maquaire, O., & Calais, E. 2002, al.). Besides, in order to detect and measure the vertical displacement or subsidence of offshore platforms, GPS is considered as the best tool to determine relative position between control stations because GPS allows us to achieve a desirable precision (i.e. +0.1ppm) that is necessary for subsidence monitoring (Leick, A., Rapoport, L., & Tatarnikov, D. (2015). L) Techniques of positioning on various time and space scales have made a lot of progress in the last decade, in particular in the field of geomorphological mapping, or in the realization of Digital Elevation Model (DEM) by numerical photogrammetry (Girault, F. 1992; Miyazawa, K., Yoshizawa, N., Onozuka, R., Hisamatu, F. 2000, Weber, D., Herrmann, A, 2000). As a result of the constantly growing technological progress in all fields of engineering, the increasing demand for higher accuracy, efficiency, and sophistication of the deformation measurements, geodetic engineers have continuously searched for better monitoring techniques and have to refine their methods of deformation analysis. The infiltration of space techniques such as GPS has opened a new dimension in data acquisition which involves offshore structures such as gas and oil platforms which are situated hundreds of kilometers offshore (Setan and Othman, 2006). A suitable technique of data acquisition has to be identified such that a high accuracy observation can be obtained and its results can be used for deformation analysis. Amiri-Simkooei, A. R., Alaei-Tabatabaei, S. M., Zangeneh-Nejad, F., & Voosoghi,

B. (2017). proposed a method that identified the unstable points of a network based on the generalized likelihood ratio (GLR) test. The method simultaneously uses the observations of two epochs called the simultaneous adjustment of two epochs (SATE) method. SATE is applicable to one-, two-, or three-dimensional deformation networks with any type of observations, including distances, angles, global positioning system (GPS) baselines, and height difference. Samsonov et al. (2017) developed a Multidimensional Small Baseline Subset (MSBAS) methodology which is a semiautomatic processing system for computing temporally dense two-dimensional, horizontal east-west and vertical time series of ground deformation from ascending and descending SAR imagery acquired by various satellites. The MSBAS was used for mapping ground deformation at the Piton de la Fournaise volcano (La Réunion Island, France) during the February 2012–April 2016 period from RADARSAT-2 data. The five volcanic eruptions that occurred during the June 2014–October 2015 period, produced over 60cm of horizontal and over 30cm of vertical ground deformation as resolved in the MSBAS-derived time series. The results which were validated with GNSS observations show the high level of accuracy provided by geodetic means of monitoring deformation despite the technological advancements in remote sensing techniques.

Background of the study

The Obasanjo library complex (Project site) a storey building was built over two decades which experiences cracks and some physical changes necessitated the conduct of this research with the aim of given the professional state of being of the structure and give necessary recommendations and suggestion so as to rescue the structure.

Materials and Methods

The level, electronic theodolite and Differential global position system (GPS) equipment were used to carryout deformation survey with the aim of assessing the state of being of the Obasanjo library complex (project site).

GPS; Global Positioning System offers advantages over conventional terrestrial methods. Intervisibility between stations is not strictly necessary, allowing greater flexibility in the selection of station locations than for terrestrial geodetic surveys Wilczyńska, I., & Ćmielewski, K. (2016). According to him, the measurements can be carried out during night or day, under varying weather conditions, which makes GPS measurements economical, especially when multiple receivers can be deployed on the structure during the survey. With the recent developed rapid static positioning techniques, the time for the measurements at each station is reduced to a few minutes (Anonym, 2002).

The work was achieved through the establishment of second order controls around the Northern, Southern, Eastern and Western side of the study area, carryout the trigonometric heighting, carryout GPS observation, process the data/results and make necessary recommendations based on the analysis made.

The methodology followed was summarized as seen in the flow chart as presented in figure 1.0 below:

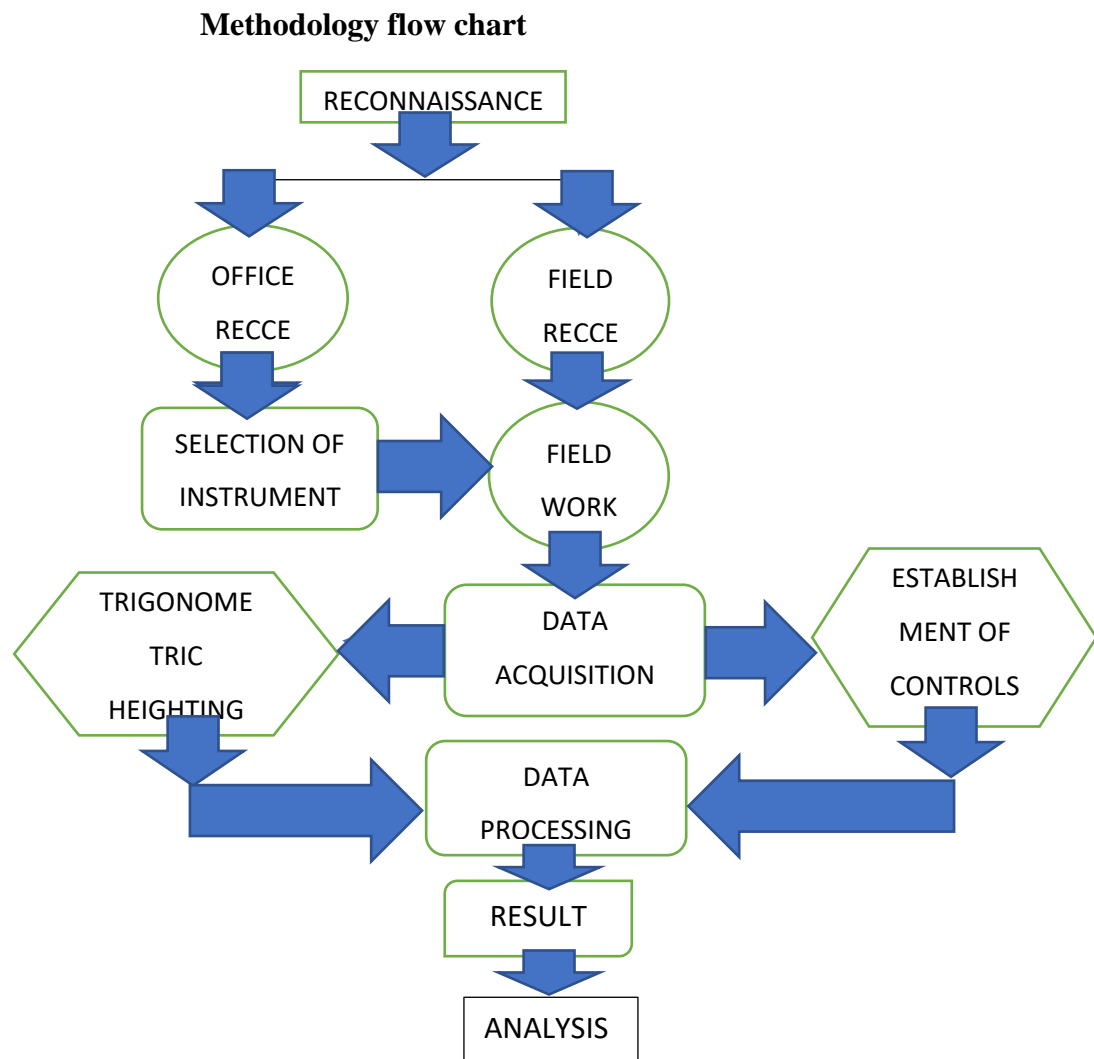


Figure 1.0 Methodology flow chat of the operation

Results and Analysis

As highlighted in the objectives, the results and Analysis are presented in form of tables and figures as seen below:

Results

Tables 1, 2, 3 and 4 present the results in form of calculations for the most probable value, standard deviation and standard errors of Northern, Southern, Eastern and Western side of the Obasanjo library complex (Project site).

NORTH - SIDE

Table 1: Calculation of standard error of the mean

Observed height (x)	(x̄ - x) = v	(x̄ - x) = v ²
9.0507	0.0000	0.0000
9.0508	-0.0001	0.00000001
9.0508	-0.0001	0.00000001
9.0508	-0.0001	0.00000001
9.0508	-0.0001	0.00000001
9.0502	0.0005	0.00000025
9.0509	-0.0002	0.00000004
9.0508	-0.0001	0.00000001
Σ = 72.4058	Σ = 0	Σ = 0.00000034

Most problem values

$$\bar{x} = \frac{\sum x}{n} = \frac{72.4058}{8} = 9.0508$$

Standard deviation

$$\begin{aligned}
 & \sqrt{\frac{\sum v^2}{(n-1)}} \\
 &= \sqrt{\frac{0.00000034}{8-1}} \\
 &= \sqrt{0.00000048} \\
 &= 0.000219089
 \end{aligned}$$

Standard error of the mean

$$\begin{aligned}
 \int m &= + \frac{s}{\sqrt{n}} = \frac{0.000219089}{\sqrt{8}} \\
 &= \frac{0.000219089}{\sqrt{8}} \\
 &= 0.0008
 \end{aligned}$$

Where : \bar{x} = mean (most problem values)

s^2 = variance

s = standard error

s_m = standard error of the mean

SOUTH – SIDE

Table 2: Calculation of standard error of the mean

Observed height (x)	(x [*] - x) = v	(x [*] - x) = v ²
9.0527	-0.0001	0.00000001
9.0525	0.0001	0.00000001
9.0529	-0.0003	-0.00000009
9.0535	-0.0009	-0.00000081
9.0525	0.0001	0.00000001
9.0520	0.0006	0.00000036
9.0524	0.0002	0.00000004
9.0525	0.0001	0.00000001
$\Sigma = 72.421$	$\Sigma = 0$	$\Sigma = 0.00000134$

Most problem value

$$\bar{x} = \frac{\sum x}{n} = \frac{72.421}{8} = 9.0526$$

Standard deviation

$$\begin{aligned}
 &\int \sqrt{\frac{\sum v^2}{(n-1)}} \\
 &= \sqrt{\frac{0.00000134}{8-1}}
 \end{aligned}$$

$$= \sqrt{0.00043752551}$$

$$= 0.02091711046$$

Standard error of the mean

$$m = \frac{s}{\sqrt{n}} = \frac{0.02091711046}{\sqrt{8}}$$

$$= \frac{0.02091711046}{\sqrt{8}}$$

$$= 0.0073$$

EAST – SIDE

Table 3: Calculation of standard error of the mean

Observed height (x)	(x̄ - x) = v	(x̄ - x) = v ²
9.0497	0.0034	0.0001156
9.0482	0.0049	0.00002401
9.0499	0.0032	0.00001024
9.0549	-0.0018	0.00000324
9.0566	-0.0035	0.00001225
9.0567	-0.0036	0.00001296
9.0524	0.0007	0.00000049
9.0566	-0.0035	0.00001225
Σ = 72.425	Σ = 0	Σ = 0.000087

Most problem values

$$\bar{x} = \frac{\sum x}{n} = \frac{72.425}{8} = 9.0531$$

Standard deviation

$$s = \sqrt{\frac{\sum v^2}{(n-1)}}$$

$$= \sqrt{\frac{0.000087}{8-1}}$$

$$= \sqrt{0.00001242857}$$

$$= 0.00352541771$$

Standard error of the mean

$$s_m = \frac{s}{\sqrt{n}} = \frac{0.00352541771}{\sqrt{8}}$$

$$= \frac{0.00352541771}{\sqrt{8}}$$

$$= 0.0012$$

WEST – SIDE

Table 4: Calculation of standard error of the mean

Observed height (x)	(x̄ - x) = v	(x̄ - x) = v ²
9.0391	-0.0007	0.00000049
9.0385	-0.0001	0.00000001
9.0386	-0.0002	0.00000004
9.0382	0.0002	0.00000004
9.0385	-0.0001	0.00000001
9.0389	-0.0005	0.00000025
9.0373	0.00011	0.00000121
9.0385	-0.0001	0.00000001
Σ = 72.3076	Σ = 0	Σ = 0.00000206

Most problem values

$$\bar{x} = \frac{\sum x}{n} = \frac{72.3076}{8} = 9.0384$$

Standard deviation

$$s = \sqrt{\frac{\sum v^2}{(n-1)}}$$

$$= \sqrt{\frac{0.00000206}{8-1}}$$

$$= \sqrt{0.00054248107}$$

$$= 0.02329122302$$

Standard error of the mean

$$\int m = + \frac{s}{\sqrt{n}} = \frac{0.02329122302}{\sqrt{n}}$$

$$= \frac{0.02329122302}{\sqrt{8}}$$

$$= 0.0082$$

Analysis

The figures 2, 3, 4 and 5 present the trend analysis plot for Northern, Southern, Eastern and Western sides of the project site where the Accuracy measures, Fitted trend equation as well as the profile of variables such as Actual, fits and forecast produced from a graph of heights against index.

For better analysis of the results obtained, the Linear Trend Model (LTM) which is the best means of interpreting the data where series of measurements were taken which shows the trend analysis plot where the Actual, Fits and Forecast were presented based on the accuracy, mean absolute percentage error (MAPE), Mean absolute deviation (MAD) and Mean square deviation (MSD) of each cardinal result as seen in figures below:

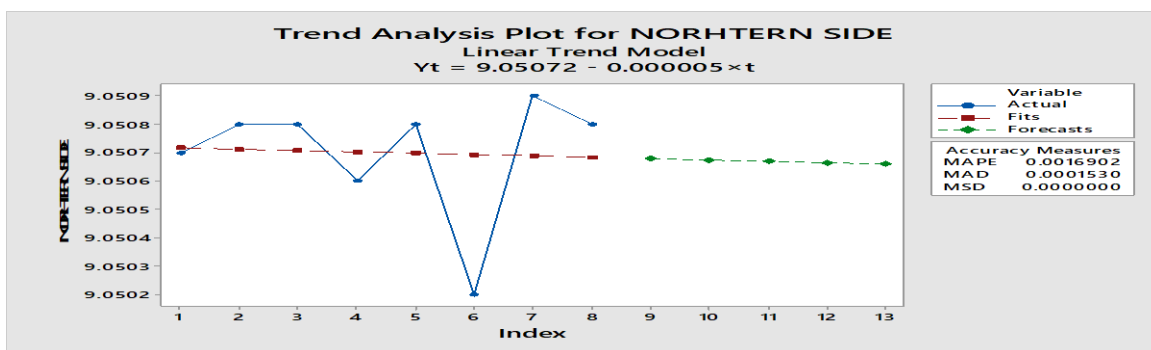


Figure 2: Trend Analysis plot for Northern side of the project site

Trend Analysis for NORHTERN SIDE

Data NORHTERN SIDE

Length 8

NMissing 0

Fitted Trend Equation

$$Y_t = 9.05072 - 0.000005 \times t$$

Accuracy Measures

MAPE 0.0016902

MAD 0.0001530

MSD 0.0000000

NORHTERN

Time	SIDE	Trend	Detrend
1	9.0507	9.05072	-0.0000167
2	9.0508	9.05071	0.0000881
3	9.0508	9.05071	0.0000929
4	9.0506	9.05070	-0.0001024
5	9.0508	9.05070	0.0001024
6	9.0502	9.05069	-0.0004929
7	9.0509	9.05069	0.0002119
8	9.0508	9.05068	0.0001167

Forecasts

Period Forecast

9	9.05068
10	9.05067
11	9.05067
12	9.05066
13	9.05066

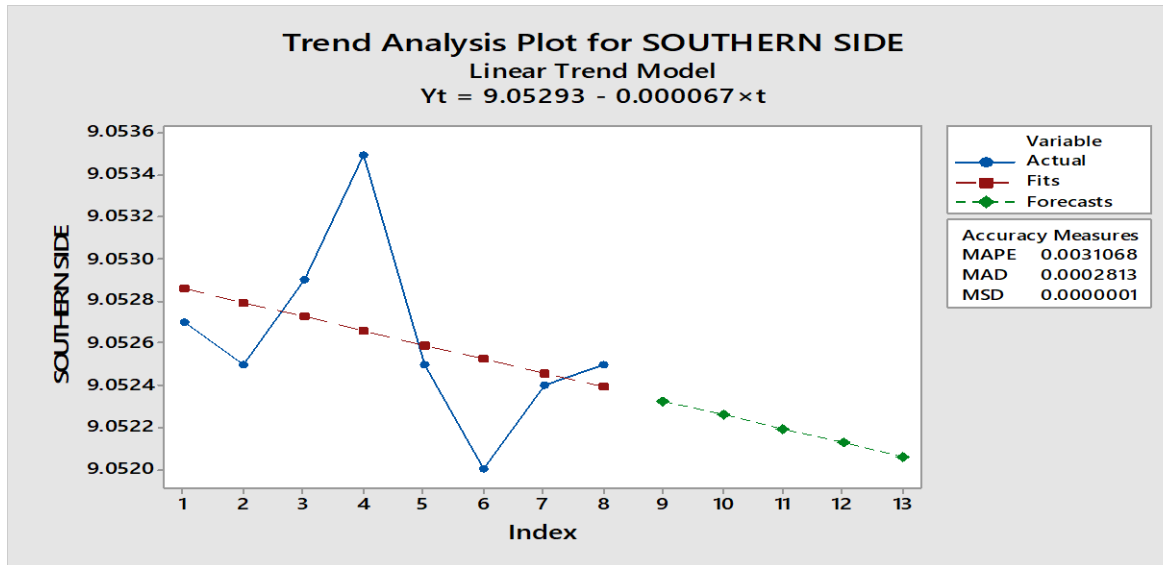


Figure 2: Trend Analysis plot for Southern side of the project site

Trend Analysis for SOUTHERN SIDE

Data SOUTHERN SIDE

Length 8

NMissing 0

Fitted Trend Equation

$$Y_t = 9.05293 - 0.000067 \times t$$

Accuracy Measures

MAPE 0.0031068

MAD 0.0002813

MSD 0.0000001

SOUTHERN

Time	SIDE	Trend	Detrend
1	9.0527	9.05286	-0.0001583
2	9.0525	9.05279	-0.0002917
3	9.0529	9.05273	0.0001750
4	9.0535	9.05266	0.0008417
5	9.0525	9.05259	-0.0000917
6	9.0520	9.05253	-0.0005250
7	9.0524	9.05246	-0.0000583
8	9.0525	9.05239	0.0001083

Forecasts

Period Forecast

9	9.05233
10	9.05226
11	9.05219
12	9.05213
13	9.05206

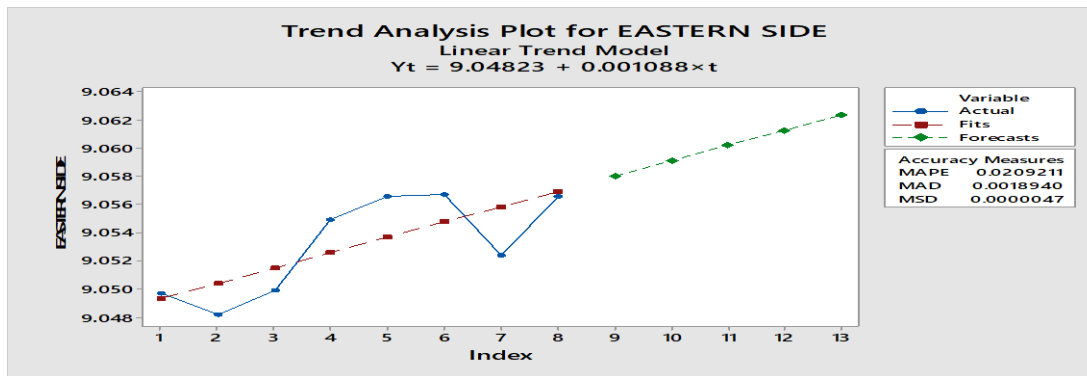


Figure 3: Trend Analysis plot for Eastern side of the project site

Trend Analysis for EASTERN SIDE

Data EASTERN SIDE

Length 8

NMissing 0

Fitted Trend Equation

$$Y_t = 9.04823 + 0.001088 \times t$$

Accuracy Measures

MAPE 0.0209211

MAD 0.0018940

MSD 0.0000047

EASTERN

Time	SIDE	Trend	Detrend
1	9.0497	9.04932	0.0003833
2	9.0482	9.05040	-0.0022048
3	9.0499	9.05149	-0.0015929
4	9.0549	9.05258	0.0023190
5	9.0566	9.05367	0.0029310

6 9.0567 9.05476 0.0019429
 7 9.0524 9.05585 -0.0034452
 8 9.0566 9.05693 -0.0003333

Forecasts

Period Forecast

9 9.05802
 10 9.05911
 11 9.06020
 12 9.06129
 13 9.06237

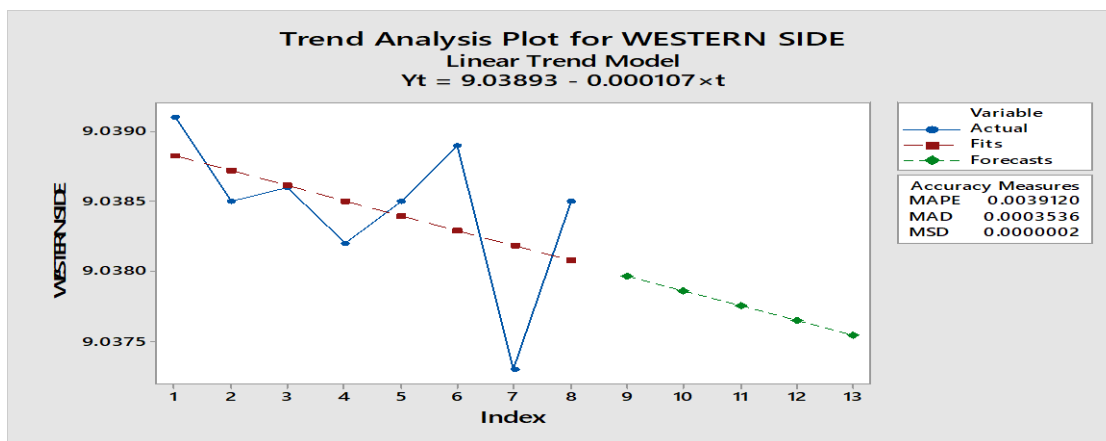


Figure 4: Trend Analysis plot for Western side of the project site

Trend Analysis for WESTERN SIDE

Data WESTERN SIDE

Length 8

NMissing 0

Fitted Trend Equation

$$Y_t = 9.03893 - 0.000107 \times t$$

Accuracy Measures

MAPE 0.0039120

MAD 0.0003536

MSD 0.0000002

WESTERN

Time	SIDE	Trend	Detrend
1	9.0391	9.03883	0.0002750
2	9.0385	9.03872	-0.0002179
3	9.0386	9.03861	-0.0000107
4	9.0382	9.03850	-0.0003036
5	9.0385	9.03840	0.0001036
6	9.0389	9.03829	0.0006107
7	9.0373	9.03818	-0.0008821
8	9.0385	9.03808	0.0004250

Forecasts

Period Forecast

9	9.03797
10	9.03786
11	9.03775
12	9.03765
13	9.03755

NOTE

(I) The **(MAPE)** express the accuracy as percentage of the error, use to compare the fit of different time series model. smaller value indicates fit.

(II) the **(MAD)** express the accuracy in some unit as the data. Smaller value indicates fit.

(III) the **(MSD)** measures the accuracy of the fitted time and the smaller value also indicate fit.

Conclusion

From the results and analysis above, it is therefore observed that the average height observed of the North, south and east of the building (study area) is relatively same because the most probable value, standard deviation and standard error are almost the same as 9.052, 0.00821 and 0.0055 respectively. Only in the case of western part that is a little bit different as the most provable value (MPV), standard deviation (SD) and standard error (SE) are 9.0384, 0.02232 and 0.0082 which indicate a little sink of 0.014m height, 0.014m MPV and 0.0027m standard error.

However, at a fitted trend equation of $Y_t = 9.0477 - 0.00031^x t$. The trend analysis plot revealed that the variables: Actual, Fits and Forecast has an average accuracy of 0.0074075 MAPE, 0.0006704 MAD Sand 0.000012 MSD.

However, even though these precautions, to provide better results in deformation analysis, GPS measurements have to be supported with Precise Levelling measurement

References

- Amiri-Simkooei, A. R., Alaei-Tabatabaei, S. M., Zangeneh-Nejad, F., & Voosoghi, B. (2017). Stability analysis of deformation-monitoring network points using simultaneous observation adjustment of two epochs. *Journal of surveying engineering*, 143(1), 04016020.
- Anonym, 2002. Structural Deformation Surveying (EM 11102-1009), US Army Corps of Engineers, Washington, DC
- Brunori CA, Bignami C, Albano M, Zucca F, Samsonov S, Gropelli G, Norini G, Saroli M, Stramondo S. 2015, 'Land subsidence, earth fissures and buried faults: InSAR monitoring of Ciudad Guzman (Jalisco, Mexico)', *Remote Sensing*, vol. 7, no. 7, pp. 8610–8630.
- Ferretti, A., Novali, F., Bürgmann, R., Hilley, G., Prati, C. 2004, 'InSAR permanent scatterer analysis reveals ups and downs in San Francisco Bay Area', *Eos Trans. AGU*, vol. 85, pp. 317–324.
- J.F.A Moore 1992 monitoring building structure, Blackie and son ltd. ISBN 0-216-93141-X USA and Canada ISBN 0-442-31 333-0
- Girault, F. 1992, Auscultation de versant instables par imagerie numé'rique. The'se Inge'nieur CNAM, Paris, vol. 193
- Leick, A., Rapoport, L., & Tatarnikov, D. (2015). *GPS satellite surveying*. John Wiley & Sons.
- Malet, J. P., Maquaire, O., & Calais, E. 2002, 'The use of Global Positioning System techniques for the continuous monitoring of landslides: application to the Super-Sauze earthflow (Alpes-de-Haute-Provence, France)', *Geomorphology*, vol. 43, nos. 1-2, pp. 33-54.
- Mazzotti, S., Lambert, A., Van der Kooij, M., Mainville, A. 2009, 'Impact of anthropogenic subsidence on relative sea-level rise in the Fraser River delta', *Geology*, vol. 37, pp. 771–774.
- Marković, M. Z., Bajić, J. S., Batilović, M., Sušić, Z., Joža, A., & Stojanović, G. M. (2019). Comparative Analysis of Deformation Determination by Applying Fiber-optic 2D Deflection Sensors and Geodetic Measurements. *Sensors*, 19(4), 844.
- Miyazawa, K., Yoshizawa, N., Onozuka, R., Hisamatu, F. 2000, 'Analytic system for landslide by different time photogrammetry: presumption of underground slide surface by analysis of surface displacement data of Hachimantai Sumikawa landslide area', *Journal of the Japan Society of Photogrammetry and Remote Sensing*, vol. 39, pp. 39 – 47
- Samsonov, S. V., Feng, W., Peltier, A., Geirsson, H., d'Oreye, N., & Tiampo, K. F. (2017). Multidimensional Small Baseline Subset (MSBAS) for volcano monitoring in two dimensions: Opportunities and challenges. Case study Piton de la Fournaise volcano. *Journal of Volcanology and Geothermal Research*, 344, 121-138.
- Setan, H. and Othman, R. 2006, 'Monitoring of Offshore Platform Subsidence Using Permanent GPS Stations', *Journal of Global Positioning Systems*, vol. 5, nos. 1-2, pp. 17-21 *South African Journal of Geomatics, Vol. 9. No. 1, February 2020*
- Uren, J. and Price, W.F. 1994, *Surveying for Engineers*, 3rd edition, The Macmillan Press Ltd.
- Weber, D., Herrmann, A. 2000, 'Reconstitution de l'é'volution gé'omorphologique de versants instables par photogrammé'trie numé'rique: l'exemple du glissement de terrain de Super-Sauze (Alpes-de-Haute-Provence, France)', *Bulletin Societe Geologique de France*, vol. 171, pp. 637 – 648.
- Wilczyńska, I., & Ćmielewski, K. (2016). Modern measurements techniques in structural monitoring on example of ceiling beams. In *Proceedings of the 3rd Joint International Symposium on Deformation Monitoring (JISDM), Vienna, Austria (Vol. 30)*.